

Study on the optimization of the mechanical properties of engineered desulfurization gypsum composites using response surface methodology

TAN Yan^{1,2}, ZHOU Lijun^{1,2}, YU Jiangtao³, XIAO Henglin^{1,2}, LONG Xiong³

(1. School of Civil Engineering Architecture and the Environment, Hubei University of Technology, Wuhan 430068, China; 2. Key Laboratory of Intelligent Health Perception and Ecological Restoration of Rivers and Lakes of Ministry of Education, Hubei University of Technology, Wuhan 430068, China; 3. College of Civil Engineering, Tongji University, Shanghai 200092, China)

Abstract: Practical applications of desulfurization gypsum are limited owing to its brittleness and low strength. To overcome these challenges, researchers have developed engineered desulfurization gypsum composites (EDGCs) by incorporating ultrahigh molecular weight polyethylene (UHMWPE) fiber and sulfoaluminate cement (SAC). The mix ratio was optimized using response surface methodology (RSM). Experimental testing of EDGC under compressive and tensile loads led to the creation of a regression model that investigates the influence of variables and their interactions on the material's compressive and tensile strengths. Additionally, microscopic morphology and hydration product composition were analyzed to explore the influence mechanism. The results indicated that EDGC's compressive strength increased by up to 38.4% owing to a decreased water-binder ratio and higher SAC content. Similarly, tensile strength increased by up to 38.6% owing to increased SAC and fiber content. Moreover, EDGC demonstrated excellent strain-hardening behavior and multiple cracking characteristics, achieving a maximum tensile strain of nearly 3%. The research findings provide valuable insights for optimizing the performance of desulfurization gypsum.

Key words: engineered desulfurization gypsum composites (EDGC); response surface methodology (RSM); interaction; compressive strength; tensile strength; strain-hardening
DOI:10.3969/j.issn.1003-7985.2025.01.008

Desulfurization gypsum, a byproduct of sulfur removal from power plant emissions, has been widely used in engineering applications such as calcium sulfate whiskers, cement retarders, and self-leveling compounds^[1-2]. However, its brittleness and low mechanical strength have limited its application in engineering^[3-4].

Received 2024-07-13, Revised 2024-10-09.

Biography: Tan Yan (1981—), female, doctor, professor, tanyan@hbut.edu.cn.

Foundation item: The National Natural Science Foundation of China (No. 51978504).

Citation: TAN Yan, ZHOU Lijun, YU Jiangtao, et al. Study on the optimization of the mechanical properties of engineered desulfurization gypsum composites using response surface methodology [J]. Journal of Southeast University (English Edition), 2025, 41 (1): 58-66. DOI: 10.3969/j.issn.1003-7985.2025.01.008.

Researchers have conducted extensive research to overcome these limitations and enhance the properties of gypsum-based composites.

Previous studies have shown that AFt ($3\text{CaO} \cdot \text{Al}_2\text{O}_3 \cdot 3\text{CaSO}_4 \cdot 32\text{H}_2\text{O}$, ettringite) crystals, formed as a primary hydration product of sulfoaluminate cement (SAC), could greatly enhance the compressive strength of the gypsum matrix^[5-6]. During hydration, hemihydrate gypsum reacted with water to produce dihydrate gypsum^[7], with the resulting crystals interlocking to enhance mechanical properties. As a result, the water-binder ratio is a crucial component of the gypsum matrix. Compared with pure gypsum, fiber-reinforced gypsum demonstrates superior overall performance^[8]. Commonly used fibers include polyethylene (PP), polyvinyl alcohol (PVA), and ultrahigh molecule weight polyethylene (UHMWPE). These fibers help reduce the brittleness of the gypsum matrix. Nevertheless, PP fiber has drawbacks, such as poor adhesion and a significant gap in its interfacial transition zone with the gypsum matrix, decreasing the matrix strength^[9]. PVA fiber has a low modulus of elasticity, which negatively impacts matrix durability^[10]. Fortunately, UHMWPE fiber is more ductile and boasts excellent mechanical properties^[11]. Therefore, UHMWPE fiber could convert the failure mode of the gypsum matrix from brittle to ductile^[12]. Most studies have focused on how single factors, rather than multiple factors, affect the mechanical properties of gypsum matrix composites.

A few studies regarding the impact of multiple factors on gypsum-based composites have also been undertaken. Zhou et al.^[13] and An et al.^[14] used the response surface methodology (RSM) to develop regression models that explore how three variables and their interactions impact the mechanical properties of desulfurization gypsum-based composites. Despite this, fewer studies have been conducted to increase the ductility of gypsum-based composites.

This study sought to validate the potential for creating gypsum-based composites that exhibit both high strength and ductility. The primary matrix material used was desulfurization gypsum, with UHMWPE fiber and SAC added to improve the ductility strength of the engineered

desulfurization gypsum composites (EDGCs), respectively. Through RSM, a quadratic polynomial regression equation was formulated to determine the impacts and their interactions of key factors, namely the water-binder ratio, UHMWPE fiber content, and SAC content. Moreover, the RSM was applied to the multi-objective optimization, and the best mix ratio was identified and validated through three experimental results. Additionally, X-ray diffraction (XRD) and scanning electron microscopy (SEM) tests were conducted to assess the effect of each influencing factor on the overall EDGC properties. The research findings offer valuable guidance for developing desulfurization gypsum-based composites.

1 Materials and Methods

1.1 Raw materials

EDGCs were crafted using desulfurization gypsum, SAC, UHMWPE fiber, water, a water reducer, and a retarder. The FDG was obtained from Hebei Litu Fine Chemical Co., Ltd. The SAC was purchased from Zhucheng Jiuqi Building Materials Co., Ltd. The UHMWPE fiber was acquired from Shanghai Tongyan Construction Technology Co. A polycarboxylic acid water reducer agent (CQJ-JSS02) and a protein retardant (CQ-SHJ01) are both white powders, with apparent densities of 0.9 and 0.6 g/cm³, respectively. The particle size distribution of the FDG and SAC is illustrated in Fig. 1, showing mean particle sizes of FDG and SAC of 25.98 and 39.63 μm , respectively. The composition of desulfurization gypsum and SAC is analyzed using an X-ray fluorescence spectrometer (XRF), with their main

components presented in Table 1. Table 2 displays the performance parameters of the UHMWPE fiber.

Table 1 Main components of desulphurization gypsum and sulphoaluminate cement

Chemical component	Mass fraction/%	
	FDG	SAC
SiO ₂	2.26	7.23
Al ₂ O ₃	0.70	18.60
Fe ₂ O ₃	0.31	4.30
CaO	38.46	45.20
SO ₃	46.06	12.40
MgO	0.71	1.35
Na ₂ O	0.06	
P ₂ O ₅	0.01	
K ₂ O	0.12	
TiO ₂		0.87
Others	11.31	10.05

Table 2 UHMWPE fiber performance parameters

Length/mm	Diameter/ μm	Strength/GPa	Density/(g·cm ⁻³)	Elastic modulus/GPa
12	25	2.9	0.97	116

1.2 Response surface experimental design

RSM is a statistical method used for creating a regression model that links experimental variables to response values^[15]. It is particularly useful for achieving multiobjective optimization.

The contents of the water reducer and retarder were 0.3% and 0.2%, respectively. The primary variables considered were the water-binder ratio, UHMWPE fiber, and SAC, denoted as *A*, *B*, and *C*, respectively. The compressive strength (*Y*₁) and tensile strength (*Y*₂) were taken as response values. To design the experiment, the Box-Behnken design (BBD) method with Design-Expert13 software was employed. This involved three factors, each with three levels and two responses. The experimental setup included 17 sets of mix ratios. A new mix ratio was designed to better assess the strain-hardening behavior of the specimen, specifically setting the water-binder ratio at 1.5%, UHMWPE content at 1.5%, and SAC content at 10%, respectively. Based on prior research^[9,12-14], the factor design and level coding were set as outlined in Table 3.

Table 3 Factor design and level coding

Level	Factor		
	<i>A</i>	<i>B</i>	<i>C</i>
-1	0.32	0.5	5
0	0.35	1.0	10
1	0.38	1.5	15

Note: *A* represents water-binder ratio; *B* represents UHMWPE fiber volume fraction; *C* represents SAC mass fraction.

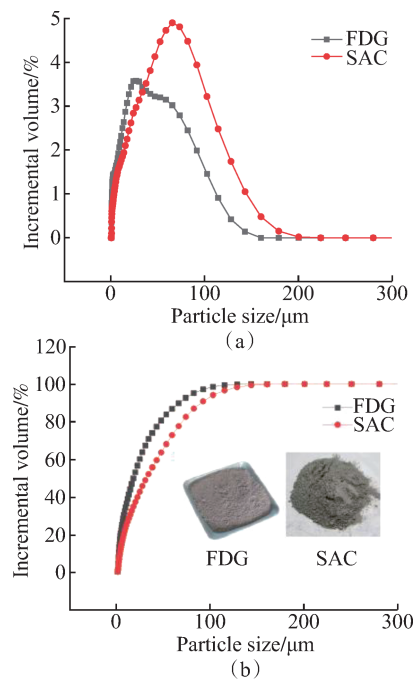


Fig. 1 Particle size distribution of FDG and SAC. (a) Particle size distribution; (b) Cumulative particle size distribution

1.3 Specimen preparation

To prepare the specimen, start by accurately weighing the mass of raw materials according to the mix ratios. Begin by adding desulfurization gypsum, SAC, a water reducer, and a retarder sequentially into a JJ5 cement sand mixer. Initially, stir these materials for 30 s, then add water to the mixture and continue stirring for an additional 60 s. Then, add the UHMWPE fiber, stirring slowly for another 60 s, followed by a fast 90 s mix to ensure a homogeneous mixture. After achieving a uniform blend, pour it into molds. Allow the specimens to set for 24 h before demolding. Cure them at a temperature of $(20 \pm 2)^\circ\text{C}$ and a relative humidity of $(60 \pm 5)\%$ for 28 d. Once the specimens reach the appropriate age, dry the specimens in an oven at 40°C until they reach a constant weight. This is followed by tests for compressive and tensile strength under dry conditions. For microscopic analysis, samples were obtained from the middle of the specimens. These samples are immersed in anhydrous ethanol for 72 h and then dried in the drying oven at 40°C . Prepare the samples for SEM by cleaning them, coating them with gold, and fixing them on copper studs using carbon tape. Finally, analyze the microscopic morphology images using the SU8010 scanning electron microscope. Additionally, for XRD analysis, grind the samples into a fine powder that passes through a 200-mesh sieve, then analyze using an Empyrean-type polycrystalline X-ray diffraction analyzer.

1.4 Test methods

The compressive strength was carried out according to Building Gypsum (GB/T 9776—2022)^[16], using $40\text{ mm} \times 40\text{ mm} \times 160\text{ mm}$ prism test molds. Each mix ratio was represented by three specimens, which were tested using the DYE-300S machine. For tensile strength, the testing adhered to the guidelines set out in the Standard Test Methods for Fiber Concrete (CECS 13: 2009)^[17]. Dog bone-shaped molds were employed, and the tests were conducted using the WDW-100C machine. Fig. 2 illustrates the dimensions of the dog bone-shaped specimen.

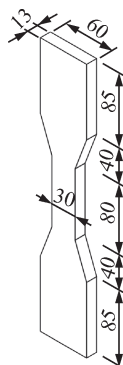


Fig. 2 Dimensions of the dog bone-shaped specimen (unit: mm)

The Hitachi scanning electron microscope was used to examine the microscopic morphology of the specimens, while the Empyrean polycrystalline XRD analyzer was utilized to analyze the hydration products.

2 Results and Discussion

2.1 Response surface model reliability analysis

Based on the principle of least squares, the response surface test results are nonlinearly fitted to obtain the Y_1 - Y_2 regression model as follows:

$$Y_1 = 79.01691 - 123.75A + 10.95B - 1.41083C - 35AB + 5.6667AC - 0.01BC \quad (1)$$

$$Y_2 = -46.085 + 289.58333A + 1.94667B + 0.2505C + 6.66667AB + 0.5AC + 0.08BC - 441.66667A^2 - 2.09B^2 - 0.0239C^2 \quad (2)$$

Table 4 lists the experimental results of EDGC.

2.1.1 Analysis of variance (ANOVA)

A P -value greater than 0.05 suggests the model is not statistically significant. A P -value between 0.0001 and 0.05 indicates the model is statistically significant, while a value less than 0.0001 shows high statistical significance^[18].

Table 5 displays the ANOVA findings of the response surface regression model for Y_1 - Y_2 . The P -value for the compressive and tensile strength were less than 0.0001, indicating that the model was highly statistically significant. This means that the fitted quadratic polynomials have high accuracy and statistical significance.

2.1.2 Correlation analysis

The model correlation is higher when the multivariate correlation coefficient (R^2) and the corrected coefficient of determination (R_{adj}^2) are close to unity (one). The difference between the predicted correlation coefficient (R_{pred}^2) and the corrected correlation coefficient (R_{adj}^2) is less than 0.2, demonstrating that the model has minimal errors and is highly accurate^[19].

The fitting accuracy of the regression model is presented in Table 6. Both R^2 and R_{adj}^2 exceed 0.96, nearly reaching unity (one). The differences between R_{pred}^2 and R_{adj}^2 for compressive and tensile strengths are 0.0562 and 0.0023, respectively. Since these differences are well below 0.2, they demonstrate the high reliability of the regression model.

2.1.3 Comparative analysis of estimated and observed values

Fig. 3 illustrates the comparison between the actual and predicted values for both compressive and tensile strengths. The test results align closely along the line $y = x$ ^[20], indicating that the regression model is highly accurate.

Table 4 Experimental results for EDGC properties

Group	Mix ratio	Variables			Response values	
		Water-binder ratio	UHMWPE fiber volume fraction/%	SAC mass fraction/%	Compressive strength/MPa	Tensile strength/MPa
1	W0.38U1S5	0.38	1	5	32.8	4.6
2	W0.35U1S10	0.35	1	10	40.9	6.1
3	W0.38U0.5S10	0.38	0.5	10	38.3	4.3
4	W0.38U1S15	0.38	1	15	40.4	5
5	W0.32U1.5S10	0.32	1.5	10	42	5.7
6	W0.35U1.5S5	0.35	1.5	5	37.3	5
7	W0.32U0.5S10	0.32	0.5	10	42.8	5
8	W0.32U1S5	0.32	1	5	41.2	5.2
9	W0.38U1.5S10	0.38	1.5	10	35.4	5.4
10	W0.35U1S10	0.35	1	10	39.9	6.1
11	W0.35U1S10	0.35	1	10	40.2	6
12	W0.35U1.5S15	0.35	1.5	15	42.6	5.7
13	W0.32U1S15	0.32	1	15	45.4	5.3
14	W0.35U0.5S5	0.35	0.5	5	38.2	4.5
15	W0.35U1S10	0.35	1	10	39.5	5.9
16	W0.35U1S10	0.35	1	10	40	6
17	W0.35U0.5S15	0.35	0.5	15	43.6	4.4

Note: W0.38U1S5 means that the water-binder ratio is 0.38, the UHMWPE fiber content is 1%, and the SAC content is 5%.

Table 5 Response surface regression model ANOVA

Response source	Compressive strength		Tensile strength	
	<i>F</i> -value	<i>P</i> -value	<i>F</i> -value	<i>P</i> -value
Model	67.55	<0.000 1	156.55	<0.000 1
<i>A</i>	207.97	<0.000 1	103.57	<0.000 1
<i>B</i>	10.87	0.008 1	371.8	<0.000 1
<i>C</i>	175.40	<0.000 1	34.71	0.000 6
<i>AB</i>	3.06	0.111 0	9.18	0.019 1
<i>AC</i>	8.01	0.017 8	5.16	0.057 3
<i>BC</i>	0.006 9	0.935 3	36.72	0.000 5
<i>A</i> ²			152.69	<0.000 1
<i>B</i> ²			263.82	<0.000 1
<i>C</i> ²			344.99	<0.000 1
Lack of fit	1.60	0.337 4	0.119 0	0.944 2

Table 6 Fitting accuracy of the regression model

Model	<i>R</i> ²	<i>R</i> _{Adj} ²	<i>R</i> _{Pred} ²	Difference
Compressive strength	0.975 9	0.961 5	0.905 3	0.056 2
Tensile strength	0.995 1	0.988 7	0.986 4	0.002 3

Note: Difference is obtained by $R_{Adj}^2 - R_{Pred}^2$.

2.2 Interaction effects for compressive strength and tensile strength

A higher *F*-value and a lower *P*-value indicate that the variable has a more significant influence on the response value^[14]. Table 5 illustrates these values, highlighting how they rank in terms of influence. For compressive strength, the ranking of single-factor influence is $A > C > B$. For interaction among factors, the ranking is $AC >$

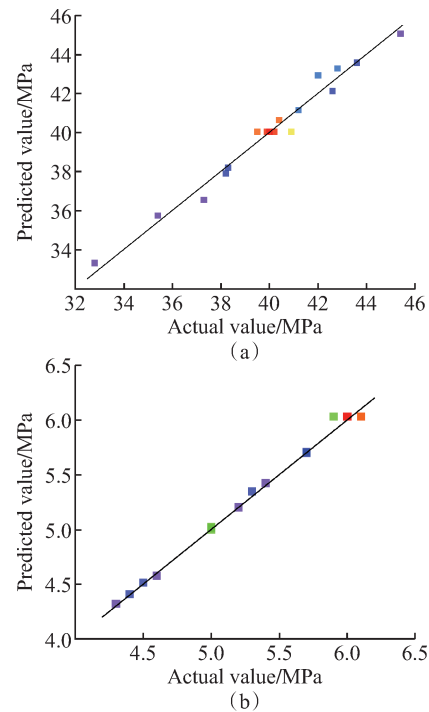


Fig. 3 Comparative analysis between the actual and predicted values. (a) Compressive strength; (b) Tensile strength

$AB > BC$. In terms of tensile strength, the single-factor influence ranks as $B > A > C$. For the interactions, the order is $BC > AB > AC$.

2.2.1 Compressive strength

Fig. 4 presents a three-dimensional surface diagram and contour map, illustrating how the interaction between the water-binder ratio and SAC affects compressive

strength, with a UHMWPE fiber content of 1%. As seen in Fig. 4(a), when the SAC content is 5%, increasing the water-binder ratio from 0.32 to 0.38 causes the compressive strength to drop from 41.2 to 32.8 MPa. Similarly, with SAC content at 15%, the compressive strength decreases from 45.4 to 40.4 MPa as the water-binder ratio increases. This trend indicates that regardless of the SAC content, a higher water-binder ratio leads to a reduction in compressive strength of the EDGC. The decrease in compressive strength is mainly attributed to the formation of a higher number of micropores within the EDGC. Although only 18.6% of water is theoretically required for gypsum hydration^[15], a higher amount of water is often added to improve fluidity and delay the setting time of gypsum in actual tests^[21]. During curing, the excess water evaporates, creating numerous micropores and microcracks in the EDGC^[22], which weaken the crystal bonds of gypsum dihydrate and reduce compressive strength. As the SAC content in the EDGC increases, the compressive strength steadily improves. This improvement is attributed to the increasing density of the EDGC matrix. SASC produces three main hydration products: AH_3 gel, C-S-H gel, and Aft crystals. The binding of gypsum dihydrate crystals with Aft crystals results in a denser structure. The micropores and microcracks in the matrix were filled with AH_3 gel and C-S-H gel, which made the matrix structure more compact and improved the compressive strength.

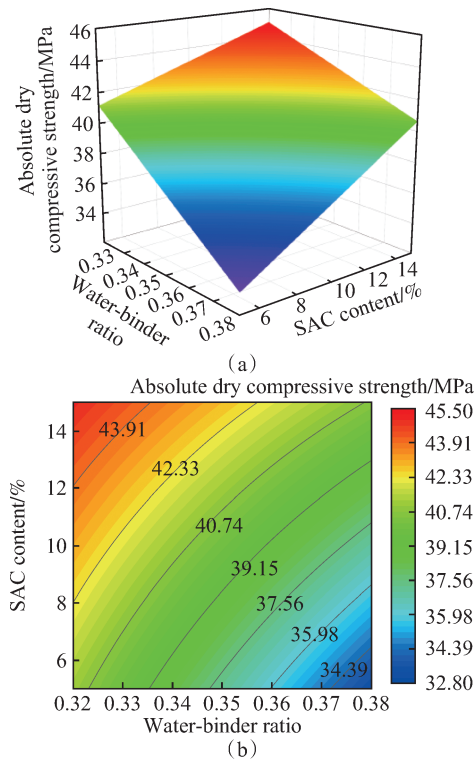


Fig. 4 Response surface diagram and contour map of the compressive strength. (a) Response surface diagram; (b) Contour map

In Fig. 4 (b), the contour map shows a distinct curve, indicating the interaction between the water-binder ratio and SAC. The minimum compressive strength ranges from a minimum of 32.8 MPa to a maximum of 45.4 MPa, indicating a significant 38.4% increase owing to this interaction. The increased SAC content mitigates the negative effect of a higher water-binder ratio on compressive strength. For instance, when the SAC content is 5%, compressive strength drops by 20.39% when the water-binder ratio rises from 0.32 to 0.38. Conversely, when the SAC content is 15%, the drop is 11.01% for the same increase in ratio. These results suggest that higher SAC levels lessen the decline in compressive strength, usually caused by increased matrix porosity from a larger water-binder ratio. A higher SAC content facilitates the production of a higher number of hydration products, which helped fill microcracks in the matrix, leading to a smaller reduction in compressive strength of the EDGC as the water-binder ratio increases.

2.2.2 Tensile strength

Fig. 5 displays a response surface diagram and contour map that illustrate how PE fiber and SAC affect the tensile strength at a water-binder ratio of 0.35. Fig. 5(a) shows that the tensile strength of the EDGC initially increases and subsequently decreases as the UHMWPE fiber content increases and the SAC content remains constant. This indicates that a proper amount of fiber en-

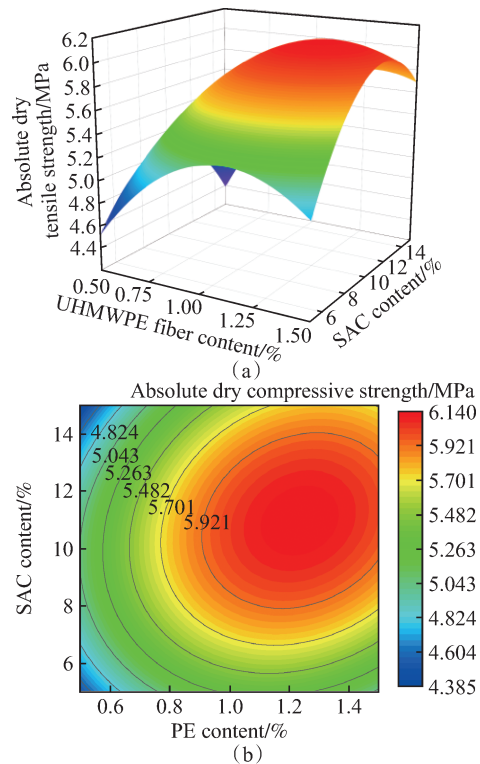


Fig. 5 Response surface diagram and contour map of the tensile strength. (a) Response surface diagram; (b) Contour map

hances the tensile strength of the EDGC owing to the fiber-matrix bridging effect, where UHMWPE fibers bond tightly with the matrix^[23]. However, an excessive amount of UHMWPE fiber may agglomerate, reducing the fiber-matrix bridging effect and, consequently, the tensile strength. Similarly, tensile strength first improves and then decreases as SAC content increases, with UHMWPE fiber content held constant. The strength was improved owing to the compact framework of the EDGC formed by the tight bonding of the hydration products of SAC and gypsum dihydrate crystals. However, an excess of AFt crystals, a type of hydration product of SAC, can produce expansion stress, loosening the framework and reducing the tensile strength of the EDGC.

Fig. 5 (b) exhibits an approximately circular shape, suggesting a notable interaction between UHMWPE fiber and SAC. The tensile strength ranges from a minimum of 4.4 MPa to a maximum of 6.1 MPa, increasing by 38.6% owing to increased SAC and fiber content and the interaction of SAC and UHMWPE fiber. This significant improvement is attributed to the fiber-matrix bridging effect, which can significantly reduce microcracking from expansion pressures^[24].

Fig. 6 shows the damage pattern and stress-strain curve diagram of the tensile specimen under different water-binder ratios (0.32, 0.35, and 0.38), with a fiber content of 1.5% and a SAC content of 10%. Figs. 6 (a) and (b) show a clear link between the number of cracks and tensile strain. Fig. 6 (b) reveals that at

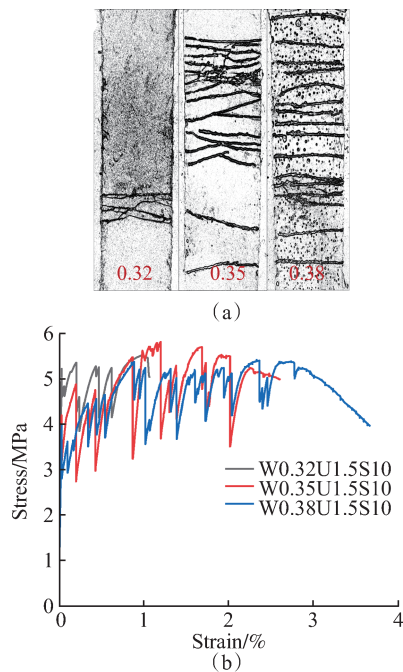


Fig. 6 Damage pattern and stress-strain curve diagram of the tensile specimen with different mix ratios. (a) Damage pattern; (b) Tensile stress-strain curve

water-binder ratios of 0.35 and 0.38, the tensile strain surpassed 2%, leading to ductile failure and demonstrating strain-hardening behavior. The maximum strain of the tensile specimen was close to 3% when the water-binder ratio was 0.38, with UHMWPE fiber content at 1.5% and SAC content at 10%. These findings demonstrate that the number of cracks and tensile strain of the specimen increase as the water-binder ratio increases. Multiple cracks occur when the fiber-matrix bridging effect overcomes the force needed to create new cracks in the matrix according to energy criteria^[12]. A lower water-binder ratio results in a denser matrix, requiring more force to form new cracks^[25]. Therefore, when the force needed for crack formation exceeds the fiber-matrix bridging effect, fewer cracks form, and the tensile strain is reduced.

2.3 Multiobjective optimization and model validation

The model was optimized using the numerical function in the Design-Expert13 software to improve the overall performance of the EDGC. The goal was to achieve excellent compressive and tensile strengths. The optimization process resulted in a compressive strength of 43.3 MPa and a tensile strength of 6.0 MPa. This was achieved with a water-binder ratio of 0.33, a UHMWPE fiber content of 1.2%, and a SAC content of 12.0%. To validate the model, three sets of parallel tests were conducted under these optimal conditions. Table 7 presents the comparison between the test values and the predicted values. The error values for compressive and tensile strengths were 1.2% and 3.3%, respectively. Both values were less than 5%, demonstrating the model's high reliability.

Table 7 Model validations

Item	Compressive strength/ MPa	Tensile strength/ MPa
Predicted value	43.3	6.0
Test value	43.9, 41.8, 42.6	5.6, 5.8, 6.1
Average value	42.8	5.8
Error/%	1.2	3.3

Fig. 7 shows the damage pattern and stress-strain curve of the tensile specimen at the optimal mix ratio (W0.33U1.2S12). As seen in Fig. 7 (a), the EDGC surface displays multiple evenly distributed cracks in the tensile zone. Fig. 7 (b) indicates that the EDGC exhibited excellent strain-hardening behavior, with a maximum tensile strength of 6.12 MPa and a maximum tensile strain of 2.89%, close to 3%. These results highlight the EDGC's high strength and toughness with the optimal mix ratio.

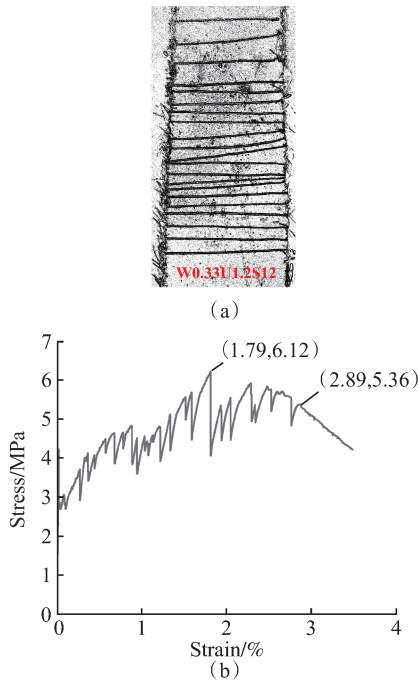


Fig. 7 Damage pattern and stress-strain curve diagram of the tensile specimen of W0.33U1.2S12. (a) Damage pattern; (b) Tensile stress-strain curve

2.4 Microscopic mechanism exploration

2.4.1 Hydration products

To examine the composition of EDGC's hydration products and the effect of different SAC contents on the EDGC properties, XRD analysis was conducted on three mix ratios: W0.35U1.5S5, W0.35U1.5S15, and W0.33U1.2S12. Fig. 8 illustrates the hydration products of EDGC for each ratio. The patterns revealed the presence of gypsum dihydrate ($\text{CaSO}_4 \cdot 2\text{H}_2\text{O}$) and AFt crystals in the hydration products. However, the C-S-H and AH_3 gels were not detected in the XRD pattern owing to their amorphous phases and low content. Zhou et al.^[13] also reached an identical inference. Notably, the mix with W0.35U1.5S15 showed higher peaks for AFt and gypsum dihydrate crystals compared to W0.35U1.5S5, suggesting improved crystallization of gypsum dihydrate crystals with increased SAC content. This increase in SAC content aligns with an increase in compressive strength. Additionally, the W0.33U1.2S12 mix exhibited taller peaks for these crystals, indicating that this op-

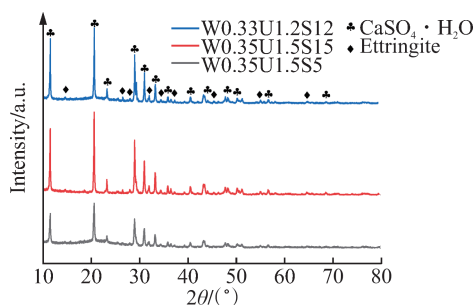


Fig. 8 Hydration products with different mix ratios

timal mix ratio boosts the mechanical properties of EDGC.

2.4.2 Microscopic morphology

To further investigate how different water-binder ratios and SAC contents affect EDGC properties, SEM analysis was conducted on five mix ratios: W0.32U1S5, W0.38U1S5, W0.35U1.5S5, W0.35U1.5S15, and W0.33U1.2S12. Fig. 9 displays the microscopic morphology with different water-binder ratios. In Fig. 9(a), corresponding to a water-binder ratio of 0.32, and Fig. 9(b), with a ratio of 0.38, both flake-shaped and plate-shaped gypsum dihydrate crystals are visible, along with microcracks on the gypsum dihydrate. Compared with the W0.32U1S5, W0.38U1S5 possessed more microcracks. This suggests that a higher water-binder ratio leads to a greater number of microcracks within the matrix, which justifies that increasing water-binder ratio decreases the mechanical strength of EDGC.

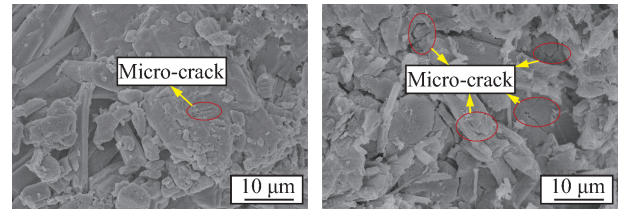


Fig. 9 Microscopic morphology with different water-binder ratios. (a) W0.32U1S5; (b) W0.38U1S5

Fig. 10 shows the microscopic morphology with different SAC contents. In Fig. 10(a), with 5% SAC content, and Fig. 10(b), with 15% SAC content, the hydration products consist mostly of gypsum dihydrate crystals with flaky and plate-like structures, AFt crystals that have needle-and-rod-like shapes, C-S-H gels with a fluffy texture, and AH_3 gels with a point-like structure. Compared with W0.35U1.5S5, W0.35U1.5S15 features a higher number of AFt crystals, C-S-H gels, and AH_3 gels. A dense structure was formed with AFt crystals and gypsum dihydrate crystals growing closely together, which directly contributes to the steady increase in the compressive strength of EDGC steadily as the SAC content rises.

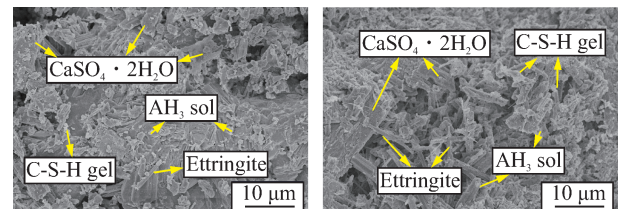


Fig. 10 Microscopic morphology with different SAC contents. (a) W0.35U1.5S5; (b) W0.35U1.5S15

Fig. 11 illustrates the microscopic morphology of W0.33U1.2S12. In this composition, gypsum dihydrate crystals and AFt crystals bound, while AH_3 and C-S-H

gels fill the microcracks in the matrix, resulting in a dense structure of EDGC, endowing it with excellent mechanical properties with the optimal mix ratio.

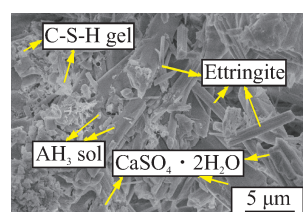


Fig. 11 Microscopic morphology of W0.33U1.2S12

3 Conclusions

(1) A multivariate quadratic regression model was created using the BBD experimental methodology to investigate how various factors and their interactions influence the compressive and tensile strengths of EDGC. Variance, correlation, and comparison analyses demonstrated that the model exhibited minimal errors and high accuracy.

(2) The study found that the compressive strength is mostly impacted by the interaction between SAC content and the water-binder ratio. This is because the major hydration products of SAC can fill the microcracks created by a higher water-binder ratio. Similarly, the tensile strength is mostly affected by the interaction between SAC and UHMWPE fibers, as the fiber-matrix bridging effect can mitigate the negative impact of the Aft crystal expansion forces.

(3) Optimization results revealed that the EDGC exhibits excellent compressive and tensile strengths at a water-binder ratio of 0.33, a UHMWPE fiber content of 1.2%, and a SAC content of 12%. Moreover, the EDGC exhibits excellent strain-hardening behavior and multiple cracking characteristics, with a maximum tensile strain of nearly 3%.

References

- [1] JIANG Y, HOU J, CHEN J F, et al. Strength characteristics of desulfurization ash-cement cured silt and application of combined curing-extraction reinforcement [J]. *Journal of Southeast University (Natural Science Edition)*, 2023, 53(3): 519-525. (in Chinese)
- [2] GERALDO R H, PINHEIRO S M M, SILVA J S, et al. Gypsum plaster waste recycling: A potential environmental and industrial solution [J]. *Journal of Cleaner Production*, 2017, 164: 288-300.
- [3] LI Y, DUAN P X, NI W, et al. Carbon footprint evaluation of cementitious materials prepared from industrial by-product gypsum based on life cycle [J]. *Silicate Bulletin*, 2023, 42(6): 1921-1930. (in Chinese)
- [4] YANG N, LI Y X, ZHAO M, et al. Modeling of direct CO₂ emission accounting for cement clinker production enterprises [J]. *Progress in Climate Change Research*, 2021, 17(1): 79-87. (in Chinese)
- [5] LIU S, LIU W, JIAO F, et al. Production and resource utilization of flue gas desulfurized gypsum in China — A review [J]. *Environmental Pollution*, 2021, 288: 117799.
- [6] LUO C R, WANG J Y, CHEN C. Current situation and analysis of industrialized comprehensive utilization of desulfurization gypsum [J]. *Coal Processing and Comprehensive Utilization*, 2023, 3: 88-100. (in Chinese)
- [7] WU Q S, MA H E, CHEN Q J, et al. Preparation of waterproof block by silicate clinker modified FGD gypsum [J]. *Construction and Building Materials*, 2019, 214: 318-325.
- [8] JIA R Q, WANG Q, FENG P. A comprehensive overview of fibre-reinforced gypsum-based composites (FRGCs) in the construction field [J]. *Composites Part B: Engineering*, 2021, 205: 108540.
- [9] ZHU C, ZHANG J X, PENG J H, et al. Physical and mechanical properties of gypsum-based composites reinforced with PVA and PP fibers [J]. *Construction and Building Materials*, 2018, 163: 695-705.
- [10] ZENG Z Y, LIAO C Q, SUN C Z. Seismic performance of high-strength concrete columns with PVA fibers in the plastic hinge zone [J]. *Journal of Southeast University (Natural Science Edition)*, 2023, 53(2): 242-251. (in Chinese)
- [11] TAN Y, LONG X, YU J T. Effects of inorganic enhancers on the mechanical, chloride ion permeation resistance and self-healing properties of PE/ECC [J]. *Journal of Composite Materials*, 2024, 41: 937-954.
- [12] WANG Y C, JIAN X R, YU J T, et al. Development of gypsum-based composites with tensile strain-hardening characteristics [J]. *Journal of the American Ceramic Society*, 2020, 103(12): 7115-7126.
- [13] ZHOU Y S, XIE L, KONG D W, et al. Research on optimizing performance of desulfurization-gypsum-based composite cementitious materials based on response surface method [J]. *Construction and Building Materials*, 2022, 341: 127874.
- [14] AN H F, WANG L L, LÜ F T, et al. Multi-objective optimization of properties on polymer fiber-reinforced desulfurization gypsum-based composite cementitious materials [J]. *Construction and Building Materials*, 2023, 369: 130590.
- [15] ZHAO B B, FANG Y, WU K. Optimized design and validation of response surface methodology for the formulation of cyanobacteria powder-penicillin sludge/low-density polyethylene composites [J]. *Journal of Composite Materials*, 2020, 37(8): 1894-1906. (in Chinese)
- [16] China Building Materials Federation. Construction gypsum: GB/T 9776—2022 [S]. Beijing: China Standard Press, 2022. (in Chinese)
- [17] Ministry of Industry and Information Technology of the People's Republic of China. Standard test methods for fibre concrete: CECS 13: 2009 [S]. Beijing: China Standard Press, 2010. (in Chinese)
- [18] LIU H H, HE Z Z, WANG Y F, et al. Preparation and analysis on graphene oxide-silver/graphene oxide/chitosan composite antibacterial dressing [J]. *Journal of*

- Southeast University (English Edition), 2023, 39(4): 416-425.
- [19] ER E, GAZIGIL L, YONAR T. Electro-oxidation of indigo blue aqueous solution for COD and color removal: RSM optimization and pilot-scale study [J]. Arabian Journal for Science and Engineering, 2024, 49(1): 415-428.
- [20] SALEH M N, BERNARDINI A T, RAMOS R A N, et al. Aural hematoma in lambs associated with *Otobius megnini* (Ixodida: Argasidae) infestation [J]. Veterinary Parasitology: Regional Studies and Reports, 2024, 47: 100944.
- [21] WAN Y, HUI X, HE X X, et al. Performance of green binder developed from flue gas desulfurization gypsum incorporating Portland cement and large-volume fly ash [J]. Construction and Building Materials, 2022, 348: 128679.
- [22] ZHOU P, XIE S L, LI Q. Analysis of the effect of water-cement ratio on concrete properties and pore structure [J]. Silicate Bulletin, 2018, 37(3): 5-14. (in Chinese)
- [23] HAMISI H, JANDE Y A C, HILONGA A. Highly reactive metakaolin: A multi-parameter optimization by response surface methodology [J]. Engineering Research Express, 2023, 5(4): 045064.
- [24] QIAN J Z, YU J C, SUN H Q, et al. Formation and role of calcite [J]. Journal of Silicates, 2017, 45(11): 1569-1581. (in Chinese)
- [25] ZHOU Y S, XIE L, ZHAO Y S. Research on sulfoaluminate cement modified desulfurization gypsum composites [J]. Nonmetallic Mining, 2021, 44(3): 17-21. (in Chinese)

响应面法优化脱硫石膏基复合材料力学性能研究

谭燕^{1,2}, 周丽君^{1,2}, 余江滔³, 肖衡林^{1,2}, 龙雄³

(1. 湖北工业大学土木建筑与环境学院, 武汉 430068; 2. 湖北工业大学河湖健康智慧感知与生态修复教育部重点实验室, 武汉 430068; 3. 同济大学土木工程学院, 上海 200092)

摘要: 脱硫石膏的力学性能较差且脆性大, 限制了其在实际工程中的应用。为改善这一缺陷, 在脱硫石膏中加入超高分子量聚乙烯(UHMWPE)纤维和硫铝酸盐水泥(SAC)制备脱硫石膏基复合材料(EDGC), 并利用响应面法(RSM)寻求其最优配合比。基于EDGC在压缩和拉伸荷载下的试验结果, 建立回归模型, 探究变量及其相互作用对EDGC抗压和抗拉强度的影响。此外, 通过微观样貌和水化产物的分析揭示其影响机理。结果表明, 水膏比的降低、SAC掺量的增加以及两者的交互作用, 促使EDGC的抗压强度提升38.4%; SAC和纤维掺量的增加以及两者的交互作用, 促使EDGC的抗拉强度提升38.6%。EDGC具有优异的拉伸应变硬化性能和多缝开裂特性, 最大拉伸应变接近3%。该研究可为脱硫石膏的性能优化与实际工程应用提供参考。

关键词: 脱硫石膏基复合材料; 响应面法; 交互作用; 抗压强度; 抗拉强度; 应变硬化

中图分类号: TB332